Nanoscale

View Online / Journal Homepage
Dynamic Article Links

Cite this: DOI: 10.1039/c2nr11906d

www.rsc.org/nanoscale

COMMUNICATION

Aligned carbon nanotubes sandwiched in epitaxial NbC film for enhanced superconductivity

Yingying Zhang,*[ab] Filip Ronning,[a] Krzysztof Gofryk,[a] Nathan. A. Mara,[a] Nestor Haberkorn,[a] Guifu Zou,[a] Haiyan Wang,[c] Joon H. Lee,[c] Eve Bauer,[a] Thomas M. McCleskey,[a] Anthony K. Burell,[a] Leonardo Civale,[a] Y. T. Zhu[d] and Quanxi Jia*[a]

Received 4th December 2011, Accepted 7th February 2012
DOI: 10.1039/c2nr11906d

Highly aligned carbon nanotube (CNT) ribbons were sandwiched in epitaxial superconducting NbC films by a chemical solution deposition method. The incorporation of aligned long CNTs into NbC film enhances the normal-state conductivity and improves the superconducting properties of the assembly.

Niobium carbide (NbC) is one of the most widely studied metal carbides since it exhibits a high melting point (3490 °C), superior hardness, and excellent chemical stability.[1,2] Furthermore, it also shows superconductivity at transition temperatures of 6.0–12.0 K.[1,3,4] As the superconducting transition temperature (T_c) of NbC is very sensitive to impurities and carbon vacancies, researchers have made great efforts to improve the superconducting properties of NbC through different approaches.[1,3–6] However, the high processing temperature (1400–2000 °C) at which NbC can be formed makes it difficult to fabricate NbC with desired properties. Carbon nanotubes (CNTs), on the other hand, have been extensively investigated due to their unique electronic properties as well as excellent mechanical strength. Particularly, an ordered CNT assembly enables new architectures, novel properties, and innovative applications.[7–12] In the past several years, both CNT fibers and ribbons have been widely investigated for different applications. For example, researchers have combined CNT fibers with other materials such as silica,[13] polymers,[14] and metal particles[15] to form composites in order to improve the mechanical strength or the electrical conductivity of the fibers. It has also been reported that CNT fibers coated with polydiacetylene can be used for electro-chromatic sensing applications.[16] Furthermore, flexible and transparent CNT ribbons have been explored for loudspeakers[17] and sources of polarized light.[18] Composites formed with CNT ribbons have been used as binder-free electrodes for batteries (combined with a monolayer of SnO_2 nanoparticles)[19] and flexible stretchable conductors (embedded in poly(dimethylsiloxane)).[20]

In this work, we report an approach to integrate CNT ribbons with epitaxial superconducting NbC films. We show that the inclusion of CNT ribbons in NbC not only enhances the normal state conductivity of the composites along the CNT axial direction, but also improves the upper critical field of NbC/CNT assembly. We further demonstrate the potential for enhanced fracture toughness of NbC/CNT composites through evidence of active toughening mechanisms during nanomechanical testing.

Fig. 1 shows the schematic diagrams for synthesizing the NbC/CNT composites. Briefly, precursor Nb solution was spin-coated on a single crystal c-cut Al_2O_3 substrate, where the Nb precursor solution was prepared by mixing $NbCl_5$ (2 g) with NH_4OH, purified water (30 ml), 20% HF (7.5 ml), and poly-ethyleneimine (PEI) (3.0 g). Detailed procedures for the preparation of precursor solutions based on such a chemical solution deposition can be found elsewhere.[21] The precursor film was subsequently annealed in ethylene at a temperature of 650 °C for 2 h, and then in forming gas (Ar + 6% H_2) at

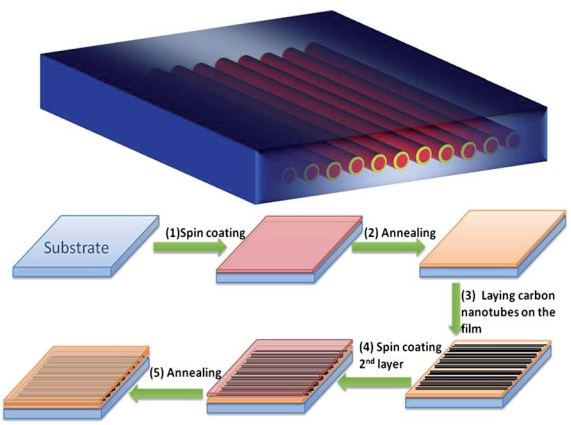

Fig. 1 Schematic illustration of the processing steps to synthesize NbC/CNT composite: (1) spin-coating precursor Nb solution on c-cut Al_2O_3; (2) annealing the precursor film in ethylene to form NbC film; (3) laying aligned CNT ribbon on the NbC film; (4) spin-coating the 2nd precursor Nb solution; and (5) annealing the composite film in ethylene and forming gas.

[a]*Division of Materials Physics and Applications, Los Alamos National Laboratory, Los Alamos, NM 87545, USA. E-mail: qxjia@lanl.gov*
[b]*Center for Nano and Micro Mechanics, Tsinghua University, Beijing, 100084, China. E-mail: yingyingzhang@tsinghua.edu.cn*
[c]*Department of Electrical and Computer Engineering, Texas A&M University, College Station, TX 77843, USA*
[d]*Department of Materials Science & Engineering, North Carolina State University, Raleigh, NC 27695, USA*

a temperature of 1000 °C for 4 h. Following that, CNT ribbon directly drawn out from the highly aligned CNT forest was laid on the surface of the NbC film. The highly-aligned CNT forest with a height about 600 μm was synthesized at 750 °C with 140 sccm forming gas (Ar + 6% H_2) and 30 sccm ethylene for 12 min.[22] The precursor Nb solution was again spin-coated on the top of the CNT ribbon and annealed using the same processing parameters as described above. It should be noted that the aligned CNT ribbon could move around during the spin-coating process. In order to immobilize the CNTs on the surface and maintain their alignment, we have pretreated the CNT ribbon with a surfactant solution before applying the second precursor Nb solution. We would like to point out that both the chemistry and the annealing temperature used to form epitaxial NbC are completely compatible with the CNT inclusions. In other words, ethylene has been used as the carbon source to synthesize both the NbC and the CNT forest, and annealing the CNT forest at 1000 °C in forming gas (Ar + 6% H_2) does not destroy CNTs.

The NbC matrix on c-cut Al_2O_3 substrate is epitaxial as demonstrated by X-ray diffraction (XRD) patterns from in-plane and out-of-plane scans. Fig. 2a shows the θ–2θ scans of the NbC/CNT film. The NbC is preferentially oriented with the (111) direction perpendicular to the substrate surface. The disappearance of CNT peaks from X-ray diffraction can be attributed to the very small quantity of CNTs in the matrix. The full width at half maximum of the (111) rocking curve is 0.85°, indicating that the NbC film (or the matrix) is well oriented normal to the substrate surface even with the inclusion of CNTs. The in-plane orientation of the NbC/CNT composite film with respect to the major axes of the c-cut Al_2O_3 substrate is measured by XRD ϕ-scans on both the NbC (200) and the Al_2O_3 (113) reflections. As shown in Fig. 2b, six peaks separated by 60° from the (200) reflections of NbC align perfectly with the peaks from (113) reflections of Al_2O_3, showing that the NbC is epitaxial with respect to the substrate. Considering the crystal structure and the lattice parameters of NbC (cubic, $a = 0.447$ nm) and Al_2O_3 (rhombohedral, $a = 0.476$ nm), this orientation relationship gives the smallest lattice misfit at the interface between the (111) oriented cubic NbC and the c-cut Al_2O_3.

The full integration of the CNT ribbon with the NbC film has been confirmed by the analysis of the micro-/nano-structures of the NbC/CNT composite films. Fig. 3a shows a top view SEM image of the aligned CNT ribbons, which were directly drawn from a well-aligned CNT (multi-walled carbon nanotube, MWNT) forest. As shown in Fig. 3a and 3b, the CNTs in the ribbon are macroscopically parallel to each other along the drawing direction, with partially wavy structures observed at a microscopic scale. Furthermore, as can be seen in Fig. 3b, the surfaces of the CNTs are very clean without any observable amorphous carbon. A high-resolution TEM image (inset in Fig. 3b) shows that the CNTs used in this study have an average diameter of around 10 nm with 4–6 walls. Fig. 3c, taken with field emission mode under an accelerating voltage of 5 kV, is a top view SEM image of the obtained NbC/CNT composite film. Although the CNTs are embedded in the NbC film, SEM is still very sensitive to the existence of CNTs due to the different electrical properties of CNTs and NbC matrix. Comparing Fig. 3a and 3c, one can clearly see that the aligned CNT ribbons are well retained after the spin-coating of Nb precursor solution and the high-temperature annealing process to convert the precursor into an epitaxial NbC matrix.

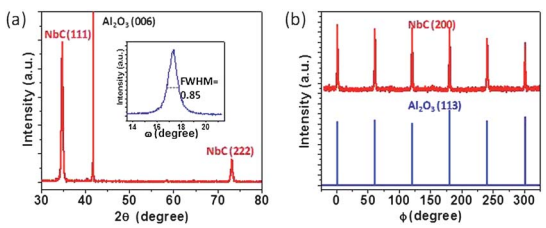

Fig. 2 X-ray diffraction patterns of the NbC/CNT composite on c-cut Al_2O_3 substrate: (a) θ–2θ scans, where inset shows the rocking curve of the (111) reflection of NbC film; (b) ϕ-scans from (200) reflection of NbC film and (113) of Al_2O_3.

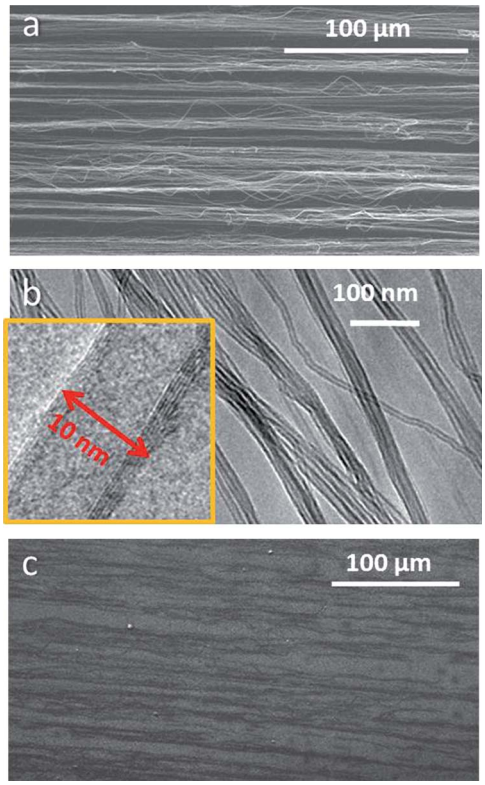

Fig. 3 SEM and TEM images of the CNT ribbons and the composite film. (a) SEM image of the CNT ribbon. (b) TEM image of the CNT ribbon and a typical high-resolution TEM image of an individual CNT (inset). (c) SEM image (top view) of the NbC/CNT composite film.

The enhanced superconducting properties of epitaxial NbC/CNT composite films in comparison with pure epitaxial NbC films are demonstrated by the upper critical field (H_{c2}, the field above which the material goes into the normal state). Fig. 4 shows the H_{c2} (H is normal to the film surface) as a function of temperature for both the pure epitaxial NbC and the NbC/CNT composite films. Inset in Fig. 4 shows the normalized resistivity at different magnetic fields as a function of temperature for a typical NbC/CNT composite film. The H_{c2} is defined as the onset field at which the $\rho/\rho_N = 95\%$, where ρ_N is the normal state resistivity right above the transition temperature. A value of H_{c2} over 4.5 T at 4.2 K for the epitaxial NbC/CNT composite, to the best of our knowledge, is the highest reported value for NbC films. In comparison, the H_{c2} of the pure epitaxial NbC film with a similar transition temperature is 30% lower in comparison with the NbC/CNT composite. A higher H_{c2} means that the composites

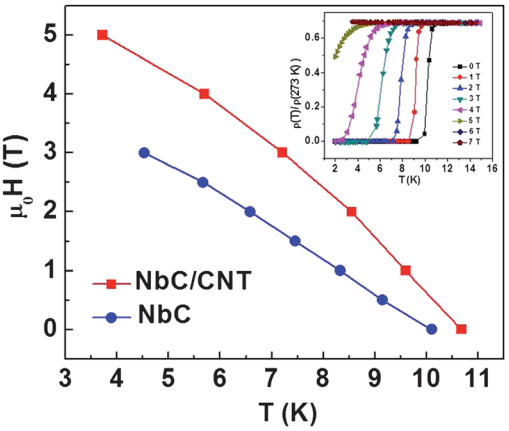

Fig. 4 Temperature dependence of the upper critical field (H_{c2}) of the NbC/CNT composite film and the pure NbC film on sapphire substrate. Inset: Normalized resistivity at different magnetic fields as a function of temperature for a typical NbC/CNT composite film. The magnetic field is applied perpendicular to the film and the resistivity is measured in the direction parallel to CNTs.

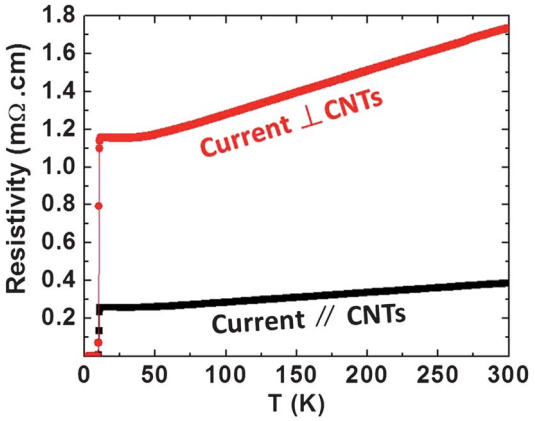

Fig. 5 Temperature dependence of the resistivities of a NbC/CNT film measured when the current is applied along different directions of the CNTs.

remain superconductive at higher magnetic field, enabling applications where magnetic field is a concern. The much enhanced H_{c2} ($H_{c2} = \Phi_0/2\pi\zeta^2$) in the NbC/CNT composite, where $\Phi_0 = hc/2e \sim 2 \times 10^{-7}$ G cm^2 is the flux quantum, indicates that the inclusion of CNT ribbons in the epitaxial NbC matrix effectively reduces the coherence length (ζ) of NbC. It should be noted that the values of H_{c2} are quite similar when the field is either perpendicular or parallel to the film surface, which is in contrast with the anisotropic H_{c2} observed from bulk NbC/CNT composites, where CNT forests with heights up to several millimetres are coated by NbC.[23] In addition, we would like to point out that the superconducting transition temperature (T_c) is slightly higher for the NbC/CNT composite film compared with the controlled pure NbC film. Typically, the T_c of NbC/CNT is around 10.5 K or above, while that of pure NbC films made by PAD with the same processing conditions is in the range of 7–10 K. It is well known that the T_c of NbC is quite sensitive to the variation of C/Nb ratio, defects, and impurities.[1,3,5,6] As our NbC/CNT film has been annealed at a temperature of 1000 °C, the carbon atom from the outer walls of CNTs can potentially contribute to a higher carbon content, which could result in a slightly higher T_c.

Another important effect of the inclusion of a CNT ribbon in an epitaxial NbC matrix is the reduction of normal state resistivity of the composite along the CNT axial direction. As discussed above, the CNT ribbons are highly aligned in the composite film. One would expect to see the anisotropic electrical resistivity when the current is flowing along different directions. Fig. 5 shows the resistivity *vs.* temperature characteristics of the NbC/CNT composite film when the current is flowing either normal or parallel to the CNT axial direction. The resistivity of the NbC/CNT composite film along the CNT axial direction is four times lower than the resistivity normal to the CNT axial direction at 300 K. The anisotropic resistivity of the NbC/CNT film at the normal state clearly indicates that one can further manipulate the electrical properties of the NbC/CNT assembly by optimizing either the amount of CNT ribbons in the composite or the length of CNTs.

Fig. 6 is a SEM micrograph of the film after nanoindentation with a Berkovich pyramidal diamond indenter to a depth of one micron. As seen in the micrograph, the film has fractured, and the CNTs protrude from the fracture surface at the edge of the film. A closer look at the corner of the indent as shown in the inset reveals evidence of CNTs bridging the propagating crack. Control of crack bridging as well as fiber pull-out is a well-known mechanism for enhanced toughness of fiber-reinforced composites.[24] While the efficacy of these methods depends on the matrix-fiber bonding strength, which is not quantified here, it does show the potential for enhancing fracture toughness through control of the fiber-matrix bond strength *via* different processing routes or use of different surfactants on the CNTs prior to embedding in the NbC matrix.

In summary, CNT ribbons have been successfully incorporated into epitaxial superconducting carbide films through a chemical solution method. The polymer solution deposition method used in this work is fully compatible with the incorporation of CNTs into other carbide films. We demonstrated that the NbC/CNT composite films show much enhanced upper critical field as compared with the pure NbC films. The inclusion of aligned CNT ribbon in an epitaxial NbC matrix not only improves the superconducting properties, but also has the potential to enhance the fracture toughness.

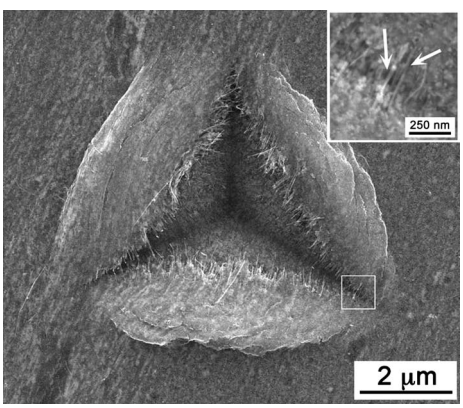

Fig. 6 SEM image of NbC/CNT after nanoindentation to a depth of 1 μm. Inset shows evidence of CNT crack bridging as marked by arrows, which is a toughening mechanism that can lead to enhanced fracture toughness.

Notes and references

1 A. L. Giorgi, E. G. Szklarz, E. K. Storms, Allen L. Bowman and B. T. Matthias, *Phys. Rev.*, 1962, **125**, 837.
2 A. A. Adamovskii, *Powder Metall. Met. Ceram.*, 2007, **46**, 595.
3 A. I. Gusev and A. A. Rempe, *Phys. Status Solidi B*, 1989, **151**, 211.
4 E. V. Pechen, S. I. Krasnosvobodtsev, N. P. Shabanova, E. V. Ekimov, A. V. Varlashkin, V. S. Nozdrin, A. M. Tschovrebov and A. I. Golovashkin, *Phys. C*, 1994, **235**, 2511.
5 J. Greek, *Radiat. Eff.*, 1980, **48**, 35.
6 D. Niculescu and E. Cruceanu, *J. Mater. Sci.*, 1985, **20**, 467.
7 K. Jiang, Q. Li and S. Fan, *Nature*, 2002, **419**, 801.
8 M. Zhang, K. R. Aktinson and R. H. Baughman, *Science*, 2004, **306**, 1358.
9 Y. Y. Zhang, L. Stan, P. Xu, H. L. Wang, S. K. Door, H. Htoon, Y. T. Zhu and Q. X. Jia, *Carbon*, 2009, **47**, 3332.
10 A. L. M. Reddy, M. M. Shaijumon, S. R. Gowda and P. M. Ajayan, *Nano Lett.*, 2009, **9**, 1002.
11 Z. P. Yang, L. J. Ci, J. A. Bur, S. Y. Lin and P. M. Ajayan, *Nano Lett.*, 2008, **8**, 446.
12 H. Zhao, Y. Y. Zhang, P. D. Bradford, Q. Zhou, Q. X. Jia, F. G. Yuan and Y. T. Zhu, *Nanotechnology*, 2010, **21**, 305502.
13 H. Peng, M. Jain, D. E. Peterson, Y. T. Zhu and Q. X. Jia, *Small*, 2008, **4**, 1964.
14 W. Ma, L. Liu, Z. Zhang, R. Yang, G. Liu, T. Zhang, X. An, X. Yi, Y. Ren, Z. Niu, J. Li, H. Dong, W. Zhou, P. M. Ajayan and S. Xie, *Nano Lett.*, 2009, **9**, 2855.
15 Q. Li, Y. Li, X. Zhang, S. B. Chikkannanavar, Y. Zhao, A. M. Dangelewicz, L. Zheng, S. K. Doorn, Q. X. Jia, D. E. Peterson, P. N. Arendt and Y. T. Zhu, *Adv. Mater.*, 2007, **19**, 3358.
16 H. Peng, X. Sun, F. Cai, X. Chen, Y. Zhu, G. Liao, D. Chen, Q. Li, Y. Lu, Y. Zhu and Q. X. Jia, *Nat. Nanotechnol.*, 2009, **4**, 738.
17 L. Xiao, Z. Chen, C. Feng, L. Liu, Z. Q. Bai, Y. Wang, L. Qian, Y. Zhang, Q. Li, K. Jiang and S. S. Fan, *Nano Lett.*, 2008, **8**, 4539.
18 M. Zhang, S. L. Fang, A. A. Zakhidov, S. B. Lee, A. E. Aliev, C. D. Williams, K. R. Atkinson and R. H. Baughman, *Science*, 2005, **309**, 1215.
19 H. X. Zhang, C. Feng, Y. C. Zhai, K. L. Jiang, Q. Q. Li and S. S. Fan, *Adv. Mater.*, 2009, **21**, 2299.
20 Y. Y. Zhang, C. J. Sheehan, J. Zhai, G. Zou, H. M. Luo, J. Xiong, Y. T. Zhu and Q. X. Jia, *Adv. Mater.*, 2010, **22**, 3027.
21 Q. X. Jia, T. McCleskey, A. Burrell, Y. Lin, G. Collis, H. Wang, A. Li and S. Foltyn, *Nat. Mater.*, 2004, **3**, 529.
22 Y. Y. Zhang, C. J. Sheehan, J. Zhai, G. Zou, H. Luo, J. Xiong, Y. T. Zhu and Q. X. Jia, *Adv. Mater.*, 2010, **22**, 3027.
23 G. F. Zou, H. M. Luo, S. Baily, Y. Y. Zhang, N. F. Haberkorn, J. Xiong, E. Bauer, T. M. McCleskey, A. Burrell, L. Civale, Y. T. Zhu, J. L. MacManus-Driscoll and Q. X. Jia, *Nat. Commun.*, 2011, **2**, 428.
24 T. L. Anderson, *Fracture Mechanics: Fundamentals and Applications*, 2nd ed. CRC Press: New York, 1995.